Experimental investigations of the nickel alloy laser melting parameters influence on porosity and surface roughness of the complex geometry products during the process of their three-dimensional formation

UDC 546.74.055

***A. V. Dub**, Professor, First Deputy Director General*[1]
***V. V. Beregovskiy**, Deputy Director General, Director of the Institute for Surface and Nanomaterials Technology (ISNT)*[2]
***E. V. Tretyakov**, Deputy Director of the ISNT for production planning work*[2]
***S. A. Shchurenkova**, Head of the Vacuum Coatings and Evacuating Equipment Laboratory*[2], *e-mail: svetastch@yandex.ru*

[1] *JSC "Science and Innovations", Moscow, Russia.*
[2] *Joint Stock Company "Research and Manufacturing Association "Central Research and Development Institute for Mechanical Engineering Technology", Moscow, Russia.*

Presented in the paper are the experimental investigations of the physical parameters (laser output power within the limits of 245-305 W, scanning speed within the limits of 605–1005 mm/s) of selective laser melting of a KhN45MVTUBR (ХН45МВТЮБР) EP-718 (ЭП-718) nickel alloy in the process of a layer-by-layer synthesis of the complex-geometry products with curved elements and honeycomb structures influence on surface roughness, dimensions and density of pores distribution in a grown layer. It is found that the porosity of the complex-geometry samples being studied in the sections parallel and perpendicular to the direction of formation, amounts to 0.58–3.18% depending on the energy density of laser irradiation value, laying within the limits of 244–504 J/m, and the surface roughness varies within the *Ra* 8.6–19.3 μm limits as well. It is determined that surface roughness depends on the energy density of laser irradiation in the same manner as a porosity does as well as pores distribution by their size for different process modes of operation. It is defined that process modes of operation based on high speeds (up to 1005 mm/s) with the linear energy density of laser irradiation of 244–303 J/m cause formation of a great number of coarse pores which appear due to instability of a molten track at high scanning speeds. The process modes of operations based on scanning speed within the 605 mm/s limits leads to increase of the small pores (up to 10 μm) quantity as the linear energy density grows up to 405–504 J/m. It is established that the optimal process mode of operations of a KhN45MVTUBR (EP-718) alloy selective laser melting (SLM) for the complex geometry parts comprises the following parameters: laser output power of 275 W, scanning speed of 605 mm/s, hatching range of 120 μm, laser spot diameter of 80 μm, powder layer thickness of 50 μm, checkerboard scanning strategy.

Key words: selective laser melting, nickel alloy, porosity, complex geometry, three-dimensional prototyping.

DOI: *10.17580/nfm.2016.12.06*

Introduction

Nickel superalloys are widely used in gas turbine engineering as blade material. Nowadays, gas turbine blades are manufactured by the labour-intensive and expensive method of casting over consumable patterns. The up-to-date method of the gas turbine blades production with the use of selective laser melting will allow to significantly reduce the price of their manufacturing, to develop new blade designs with more advanced and efficient cooling system, which guarantees an intensive heat abstraction and allows blading to work at elevated gas temperatures and thus to increase an efficiency factor of gas turbine engines. To achieve this, it is necessary to fulfill a great number of investigations focused on determination of the optimal physical parameters and SLM process technological maps, allowing to obtain products of high quality which meet the requirements to uniformity, surface roughness, porosity, strength and other characteristics [1]. In the present paper, choice of the optimal physical parameters of a KhN45MVTUBR (EP-718) nickel alloy SLM has been made along with the study on their influence on roughness and porosity in the process of a layer-by-layer growing of the complex geometry products.

Theoretical grounds

Two types of porosity are classified on microstructure observation of the products obtained by SLM method as follows: regular spherical pores and irregular pores. Microscopical examination of the powder cross thin sections has shown that most particles have regular spherical form, but particles of irregular form also occur, and at the same time, small spherical pores formed by gas capture during spraying are presented in some powder particles [2]. Pores of irregular form customary as a rule arise in powder particles of irregular form due to a collision of the incompletely hardened powder particles. Therefore, porosity and pores form of already alloyed samples can be derived from the powder, which explains an appearance of relatively small (1–5 μm) pores. Arising of coarse pores depends on the SLM process parameters to a greater extend [2].

Many researchers explain the defects formation by the limit of Plateau – Rayleigh capillary instability for a liquid cylinder [3–5]. In other words, when high scanning speed and low laser power make conditions for arising of a circular cylinder of a liquid torn loose from substrate, the track stability starts to depend on such parameters as diameter and length of the molten track [3, 6]. Insufficient laser power or high scanning speed can lead to the significant surface roughness augmentation, which in its turn can cause the pores formation [7]. Such defects can result in appearance of coarce vertical pores up to 14 layers in spread [8, 9].

On the whole, as the investigations show [7, 10, 11], the main parameter affecting the pores formation for the most part is linear energy density of laser irradiation, supplied to the powder surface. This parameter consists of the laser power and scanning speed and is determined by the formula (1)

$$\eta = P/V, \qquad (1)$$

where η — linear density of laser emission, J/m; P — laser power, W; V — scanning speed, m/s.

Description of experiments

To study how the SLM parameters of a KhN45MVTUBR (EP-718) nickel alloy powder effect on geometry and density of pores distribution in the manufactured article layer being grown, the experimental samples with curved elements and honeycomb structures of complex geometry has been made (Fig. 1). Surface roughness has been examined on flat samples of 30×40×1 mm size,

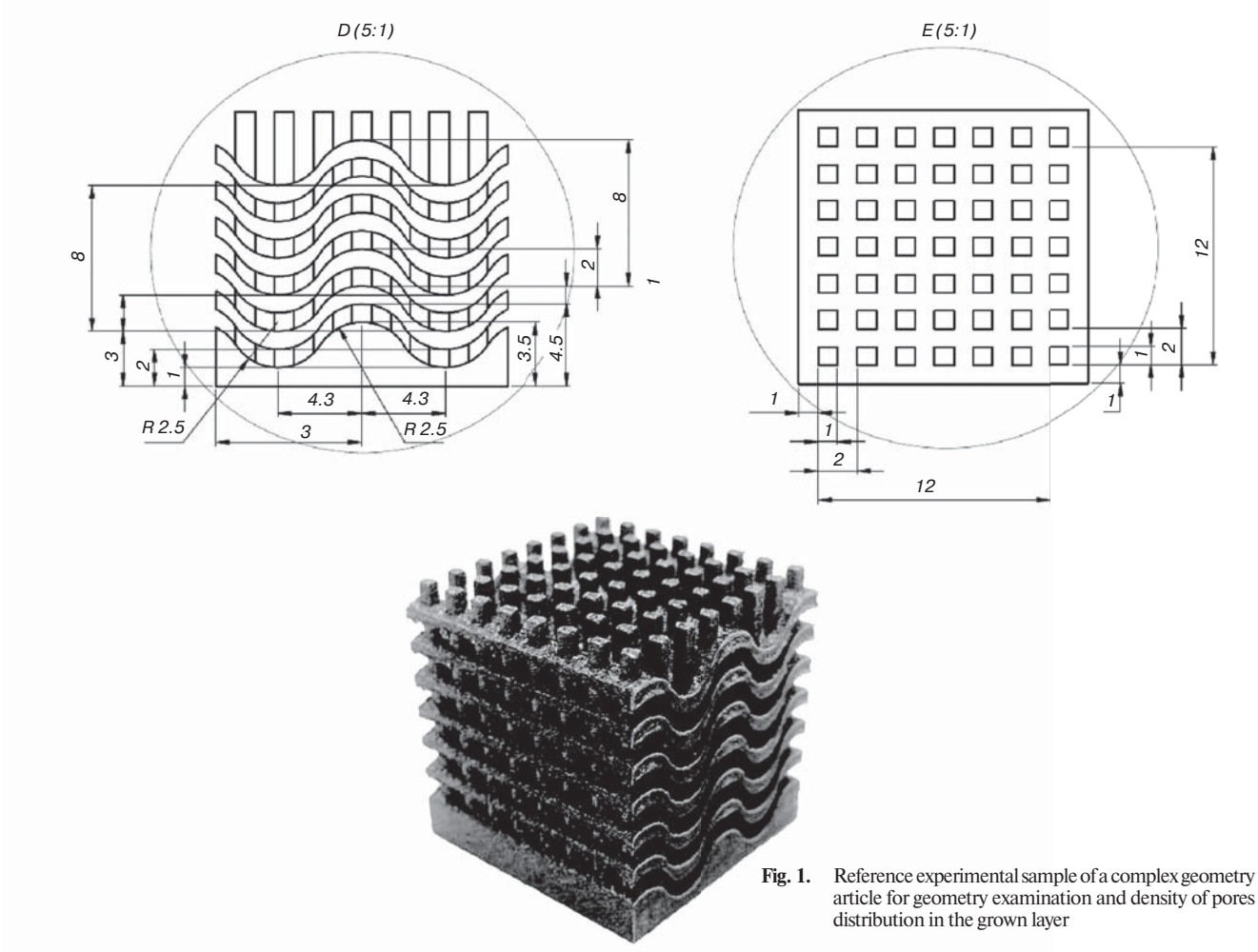

Fig. 1. Reference experimental sample of a complex geometry article for geometry examination and density of pores distribution in the grown layer

Table 1

The laser power and scanning speed values of 5 different technological modes for material of EP-718 type

Mode	KhN45MVTUBR (EP-718)		
	P, W	*V*, mm/s	η, J/m
1	275	805	342
A1	245	605	405
A2	245	1005	244
B1	305	605	504
B2	305	1005	303

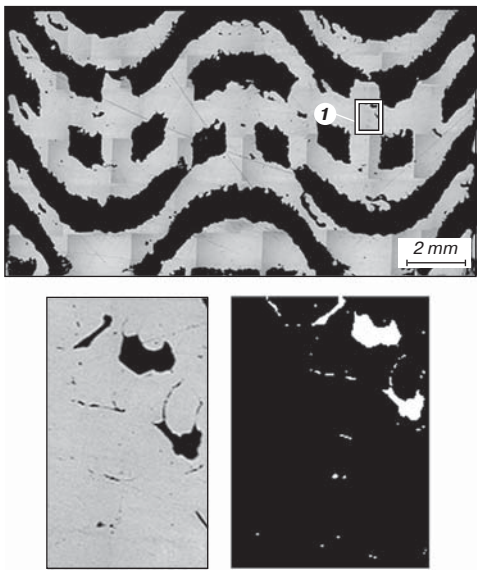

Fig. 2. Microsection panorama of a complex geometry sample obtained according to the process mode of operation No. 1 perpendicular to the direction of construction (upper image); the segment 1 with pores (bottom image) and result of its processing in Image Expert software, ×50

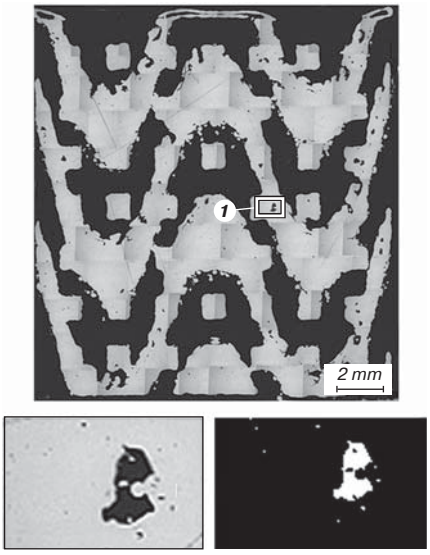

Fig. 3. Microsection panorama of a complex geometry sample obtained according to the process mode of operation No. 1 parallel to the direction of construction (upper image); the segment 1 with pores (bottom image) and result of its processing in Image Expert software, ×50

produced of a KhN45MVTUBR (EP-718) nickel alloy powder by SLM.

The experimental samples have been manufactured on a SLM 280 H selective laser melting unit [12] under the following physical parameters of the process:

– laser power and scanning speed have been varied within the limits of 245–305 W and 605–1005 mm/s, respectively;

– powder layer thickness has been fixed as 50 μm;

– laser spot diameter has amounted to 80 μm;

– hatching interval equal to 120 μm has been selected;

– an island (checkerboard) scanning strategy has been applied.

In Table 1, five different combinations of laser power and scanning speed selected for investigation of the laser treatment parameters effect on microstructure of the SLM manufactured articles are tabulated.

Two metallographic thin sections, parallel and perpendicular to the article manufacturing direction (*Z* axis) has

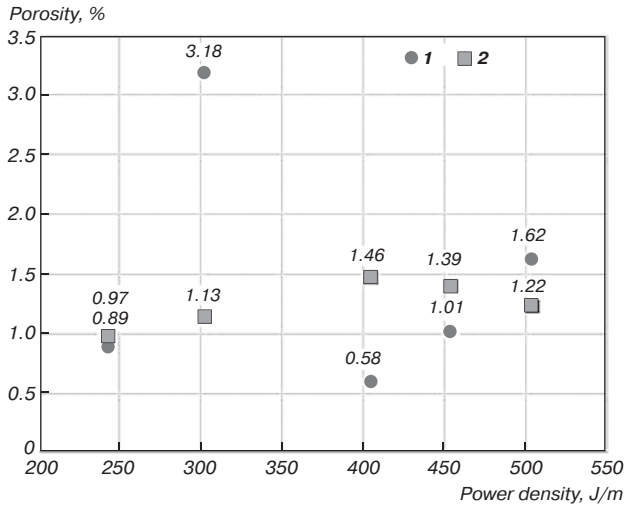

Fig. 4. Porosity dependence on linear power density for a complex geometry sample
1 — *X* – *Y*; *2* — *Y* – *Z*

Table 2

Average porosity values of a complex geometry sample depending on the density of energy, supplied to the sample surface by laser emission

Plane	Mode	Energy density, J/m	Squar of pores, mm^2	Square of analysis, mm^2	Porosity, %
X – *Y*	1	342	0.214	21.1	1.01
	A1	405	0.152	26.0	0.58
	A2	244	0.166	18.6	0.89
	B1	504	0.152	9.4	1.62
	B2	303	0.369	11.6	3.18
Y – *Z*	1	342	0.153	11.0	1.39
	A1	405	0.213	14.6	1.46
	A2	244	0.154	15.8	0.97
	B1	504	0.129	10.6	1.22
	B2	303	0.148	13.1	1.13

been made for each sample. To achieve high cut accuracy relative to the *Z* axis, a Chmer AW5S electric erosion wire-cut numerical control machine has been used.

In order to determine porosity, geometry of pores and their distribution by size, panoramic survey of the whole surface of unetched sample has been carried out on a Carl Zeiss Axio Observer D1m inverted-stage metallographic microscope at ×50 magnification (Fig. 2, 3). The received image has been loaded to Image Expert software for quantitative and qualitative metallography. For porosity determination, 10 areas has been marked out in random order and then processed by Image Expert software. At the output of the program, values of the total square of analysis; square, occupied by pores; porosity (the pores square to analysis square ratio) and the number of analyzed pores have been obtained for each of 10 segments. As a result of the data file summarizing, average porosity values of samples have been defined subject to the density of energy, supplied to the sample surface by laser emission (Fig. 4). Results of the image program processing are summarized in Table 2.

For detailed scanning tracks analysis by the light microscopy methods, examinations of experimental samples have been implemented on etched thin sections (Fig. 5)

In Fig. 6 are shown the distribution diagrams of pore sizes by their relative number in the investigated samples.

Surface roughness of reference measuring templates measurements have been fulfilled on a PCE-RT 1200 profile meter with measurement accuracy up to ±10% in compliance with GOST 2789-73 Russian State standard (ГОСТ 2789–73). Values of the *Ra* parameter of sample surface, obtained under different process modes of operation are accumulated in Table 3.

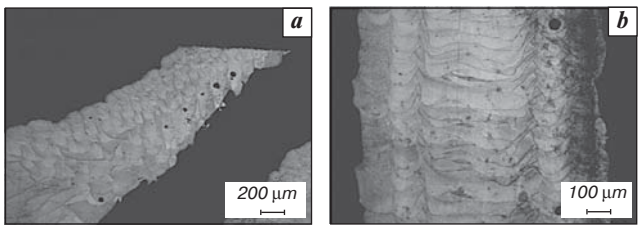

Fig. 5. Spherical gas pores, situated along the edge of the reference experimental samples

Table 3

Values of the *Ra* parameter of sample surface, obtained under different process modes of operation

Mode	Density of laser emission energy, J/m	Roughness Ra, μm
1	342	8.6
A1	405	10.5
A2	244	18
B1	504	12.0
B2	303	19.3

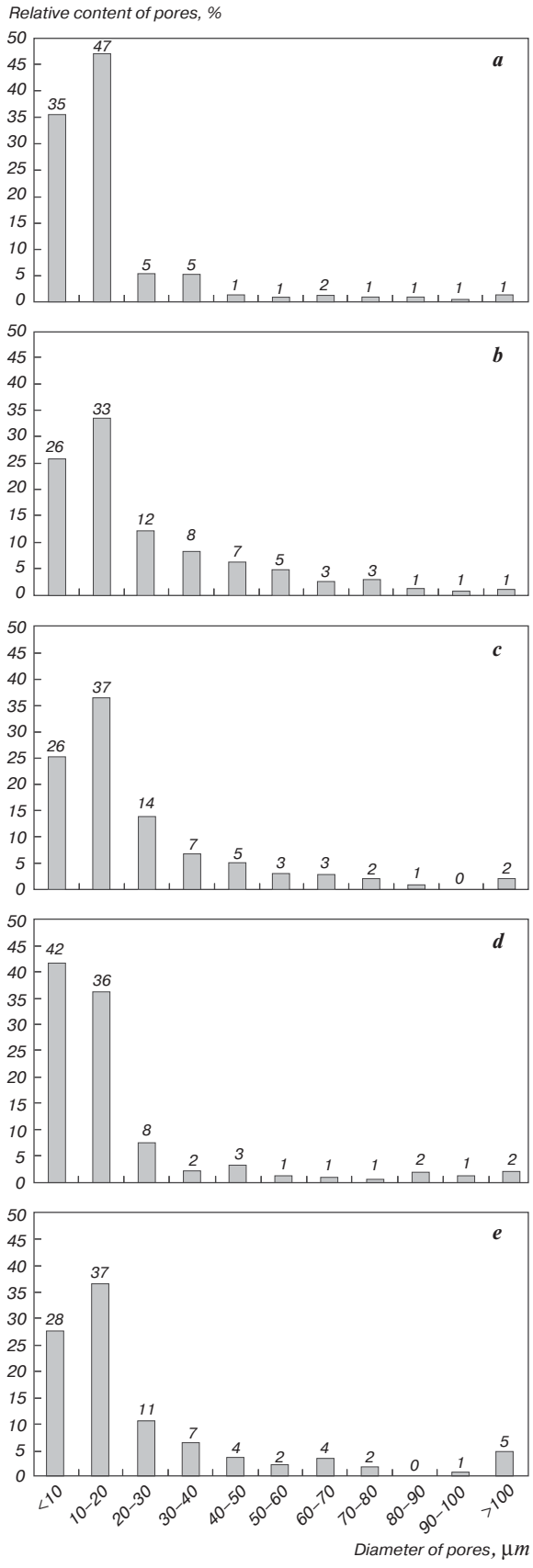

Fig. 6. Pores distribution according to their sizes under different process modes of operation:
a – 1; *b* — A1; *c* — A2; *d* — B1; *e* — B2

Consideration of results

Analysis of the implemented investigations (Fig. 2–5) allows to make the following conclusions.

1. The B2 process mode of operation with linear energy density of J/m on the complex geometry samples leads to formation of the worst porosity among all the studied ones. It is probably concerned with the given high scanning speed of the B2 mode, which can cause the molten track destabilization under certain conditions, as it is documented in literature.

2. Most often, pores arise in weak points of samples and nearby the edge.

3. On the etched thin sections images (Fig. 5) one can see that spherical gas pores are located in the center or at the bottom of scanning tracks. This can take place since at each layer scanning, the scanator firstly scans the part profile and then begins to fulfill the main volume (Fig. 5, *b*). So, a lack of material can originate in the places where the tracks of primary hatching adjoin the contour track, which can lead to a pore appearance.

4. The process modes of operation based on high scanning speeds (A2, B2) with the linear energy density of laser irradiation of 244 and 303 J/m result in formation of a large portion of coarse pores, which appears because of the molten track instability at high scanning speeds.

5. The process modes of operation with a scanning speed of 605 mm/s in foundation (A1, 1, B1), lead to increase of small pores (up to 10 μm) number as the linear energy density grow until 405, 455, 504 J/m.

6. The best figures of the pore size distribution (that is small number of coarse irregular pores) demonstrate samples, obtained under the process modes of operation No. 1 (Fig. 6).

7. The nature of surface roughness dependence is similar to that of porosity and the pore size distribution for different process modes of operation. In the given case, the mode permissive to obtain the articles with the least porosity provides also the best surface quality.

Conclusions

Thus, combination of the figures of total porosity and pores distribution by size (Fig. 4, 6) allows to assert that the optimal process mode of operation for selective laser melting of a KhN45MVTUBR (EP-718) alloy in case of the complex geometry parts comprises the following parameters: laser output power of 275 W, scanning speed of 605 mm/s, hatching range of 120 μm, laser spot diameter of 80 μm, powder layer thickness of 50 μm, checkerboard scanning strategy.

The work was performed with financial support of the Ministry of Education and Science of the Russian Federation (the unique identifier of the applied scientific research is RFMEFI57915X0125).

References

1. Beregovskiy V. V., Tretyakov E. V., Shchurenkova S. A. Oborudovanie dlya posloynogo izgotovleniya slozhnoprofilnykh izdeliy metodom selektivnogo lazernogo plavleniya MeltMaster3D 550 (Equipment for layer-by-layer manufacturing the profilecomposite articles by the MeltMaster3D 550 selective laser melting method). *Materialy II mezhdunarodnoy konferentsii "Additivnye tekhnologii: nastoyashcheye i budushcheye"* (Materials of II International conference "Additive technologies: the present and the future"). Moscow, 2016.

2. Carter L. N., Martin C., Withers P. J., Attallah M. M. The influence of the laser scan strategy on grain structure and cracking behaviour in SLM powder-bed fabricated nickel superalloy. Journal of Alloys and Compounds. 2014. Vol. 615. pp. 338–347.

3. Yadroitsev I., Gusarov A., Yadroitsava I., Smurov I. Single track formation in selective laser melting of metal powders. Journal of Materials Processing Technology. 2010. Vol. 210. pp. 1624–1631.

4. Yadroitsev I., Bertrand Ph., Smurov I. Parametric analysis of the selective laser melting process. Applied Surface Science. 2007. Vol. 253. pp. 8064–8069.

5. Gusarov A. V., Yadroitsev I., Bertrand P., Smurov I. Heat transfer modelling and stability analysis of selective laser melting. Applied Surface Science. 2007. Vol. 254. pp. 975–979.

6. Chandrasekhar S. Hydrodynamic and Hydromagnetic Stability. New York : Dover Publications, 1981. 652 p.

7. Xin Zhou, Dianzheng Wang, Xihe Liu, Dan Dan Zhang, Shilian Qu, Jing Ma, Gary London, Zhijian Shen, Wei Liu. 3D-imaging of selective laser melting defects in a Co – Cr – Mo alloy by synchrotron radiation micro-CT. Acta Materialia. 2015. Vol. 98. pp. 1–16.

8. Jianyin Chen, Lijue Xue. Process-induced microstructural characteristics of laser consolidated IN-738 superalloy. Materials Science and Engineering A. 2010. Vol. 527. pp. 7318–7328.

9. Kim I. S., Choi B. G., Hong H. U., Yoo Y. S., Jo C. Y. Anomalous deformation behavior and twin formation of Ni-base superalloys at the intermediate temperatures. Materials Science and Engineering A. Vol. 528. 2011. pp. 7149–7155.

10. Qingbo Jia, Dongdong Gu. Selective laser melting additive manufacturing of Inconel 718 superalloy parts: Densification, microstructure and properties. Journal of Alloys and Compounds. 2014. Vol. 585. pp. 713–721.

11. Investigations on the microstructure and crack formation of IN738LC samples processed by selective laser melting using Gaussian and doughnut profiles. Materials and Design. 2016. Vol. 89. pp. 770–784.

12. SLM Metal Powder. Discover the variety. SLM-Solutions. [Electronic resource] : http://slm-solutions.com/sites/default/files/attachment/page/2016/01/151023_slm_metal_powder.pdf

NFM